

Accuracy of Wind Observations from Open-Ocean Buoys: Correction for Flow Distortion

MICHAEL SCHLUNDT,^a J. THOMAS FARRAR, SEBASTIEN P. BIGORRE, ALBERT J. PLUEDDEMANN, AND ROBERT A. WELLER

Woods Hole Oceanographic Institution, Woods Hole, Massachusetts

(Manuscript received 8 August 2019, in final form 28 January 2020)

ABSTRACT

The comparison of equivalent neutral winds obtained from (i) four WHOI buoys in the subtropics and (ii) scatterometer estimates at those locations reveals a root-mean-square (RMS) difference of 0.56–0.76 m s^{−1}. To investigate this RMS difference, different buoy wind error sources were examined. These buoys are particularly well suited to examine two important sources of buoy wind errors because 1) redundant anemometers and a comparison with numerical flow simulations allow us to quantitatively assess flow distortion errors, and 2) 1-min sampling at the buoys allows us to examine the sensitivity of buoy temporal sampling/averaging in the buoy–scatterometer comparisons. The interanemometer difference varies as a function of wind direction relative to the buoy wind vane and is consistent with the effects of flow distortion expected based on numerical flow simulations. Comparison between the anemometers and scatterometer winds supports the interpretation that the interanemometer disagreement, which can be up to 5% of the wind speed, is due to flow distortion. These insights motivate an empirical correction to the individual anemometer records and subsequent comparison with scatterometer estimates show good agreement.


1. Introduction

Knowledge of the global wind field is crucial for modeling societally important oceanographic phenomena, such as ocean currents, surface waves, and regional climate modes such as El Niño. During the last four decades several global wind observation datasets have become available from satellites using radiometers and scatterometers. All of them have in common the fact that they do not observe the wind, but instead measure related parameters like brightness temperature or backscattered radiation. These parameters are related to the small-scale surface roughness, which is in turn related to the surface stress, and are finally converted to winds via a geophysical model function (GMF). For the development of the GMF, direct in situ observations are essential,

and observations from buoys are critical for providing a baseline for winds over the open ocean.

The characterization of errors in in situ measurements is critical to understanding wind-driven processes as well as evaluating remotely sensed winds from satellite. Error sources are myriad, but here are grouped into three main categories: errors inherent to the instrument, errors associated with the platform, and sampling errors. The accuracy of the measurement is dependent on sensor accuracy, sensor location, and sampling methodologies. Sensor errors are usually estimated and provided by the manufacturer. Platform related errors are of particular interest because they often result in measurement bias. These biases are related to the performance of the sensor in the deployed environment; hence, for wind sensors on a buoy at the ocean surface there can be, for example, compass errors due to the local magnetic field or flow distortion caused by the buoy superstructure. Sampling errors can arise from incomplete sampling of the measured parameter, and can be caused by discrete sampling or by the spatial or temporal averaging that is inherent in a measurement technique.

This paper focuses on understanding the performance of wind sensors on surface buoys. The Woods Hole Oceanographic Institution (WHOI) Upper Ocean

 Denotes content that is immediately available upon publication as open access.

^a Current affiliation: GEOMAR Helmholtz Centre for Ocean Research Kiel, Kiel, Germany.

Corresponding author: M. Schlundt, mschlundt@geomar.de

Processes (UOP) Group has maintained several moored buoys in the Pacific and Atlantic Oceans for almost two decades. The buoys used in this study are well maintained and are equipped with redundant meteorological instruments. The temporal resolution of the meteorological data is 1 min, and the measurement height is about 3 m above the sea surface on the buoy tower. In the case of wind measurements, a minimum of two anemometers are mounted on the buoys. Colbo and Weller (2009) analyzed and described the errors from the wind observations made on UOP buoys. The precision of the wind speed sensor is 0.002 m s^{-1} with a total error of 0.1 m s^{-1} . The wind direction measurement has a precision of 0.1° and a total instant error of about 6° . Both total errors can be higher for very low wind speed conditions.

A large vane is fixed to the leeward side of the tower on the buoy with the intention of controlling the orientation of the buoy with respect to the wind and keeping the forward face of the tower, where anemometers and temperature and humidity sensors are mounted, facing into the wind. It is notable that deployments showed a bistable orientation of the buoy, tending to divert about 30° in either direction from the head-on wind, indicating that the vane on the tower did not steer the forward face of the buoy tower directly into the wind. Opposing the steering action of the vane are the wind forces on the tower structure and the sensors and also on the watertight storage well in the center of the buoy, which houses batteries and dataloggers; the top of the well extends about 15 cm above the buoy deck and is covered by a hatch.

As part of the quality control work on the buoy data, observations from the redundant anemometers of each buoy are compared, and some differences have been noted. A computational fluid dynamics (CFD) study of the buoy type that the UOP group has been using since around 2004 (Emond et al. 2012) suggested the two anemometers could disagree by up to 5% of the wind speed. This CFD study also revealed an asymmetry in wind speeds of the port and starboard sensors, when investigating the flow distortion with oblique winds. However, it has to be mentioned that the CFD simulations were done for an idealized setting, with no wave motion or tilt on the buoy. An experiment in the Gulf Stream showed wind speed and direction discrepancies between sensors at different locations on the buoy tower consistent with the predictions of the flow distortion study, and it also showed a dependence of the inter-anemometer disagreement on the angle between the wind and the buoy's wind vane (Bigorre et al. 2013).

To quantify biases and to bring the results in relation to other wind observations, the buoy observations were

compared with two scatterometer datasets. Scatterometers have many sources of wind measurement biases that are well documented (e.g., Stoffelen and Portabella 2006; de Kloe et al. 2017; Verhoef et al. 2017). However, these biases are not believed to be variable on a global scale, that is, they are relatively stable over the investigated analysis period (Ricciardulli and Wentz 2015), a property we will exploit here to get further insights into the buoy errors caused by flow distortion.

The first scatterometer we use, operational from 1999 until 2009 in Ku band, is NASA QuikSCAT (Lungu and Callahan 2006) with its most current GMF: "QuikSCAT Ku-2011" (Ricciardulli and Wentz 2015). Neglect of a sea surface temperature (SST) dependency in the wind stress relationship can be a large error source (see, e.g., Wang et al. 2017b). Generally, pencil-beam scatterometers, like QuikSCAT, can have systematic wind direction biases, as shown, for example, by Stoffelen and Portabella (2006). The second scatterometer is ASCAT, which is a EUMETSAT project and operating in C band (Figa-Saldaña et al. 2002). This frequency band is less influenced by rain than the Ku band (Weissman et al. 2012). Currently, three ASCAT (ASCAT-A, ASCAT-B, and ASCAT-C) scatterometers are in orbit.

The differences between scatterometer and in situ wind speeds on regional scales can be large for both described scatterometer missions. Ricciardulli and Wentz (2015) estimated a root-mean-square (RMS) difference for 30-min collocations over 5 years between the used QuikSCAT dataset and a variety of buoys of 0.87 m s^{-1} with only a marginal bias of -0.03 m s^{-1} . For ASCAT they estimated an RMS of 1.11 m s^{-1} with no bias (-0.01 m s^{-1}). A few publications provided RMS differences as well. Yu and Jin (2012) found an RMS of 0.66 m s^{-1} for the whole QuikSCAT period using a large set of daily averaged buoy observations. Freilich and Dunbar (1999) found an RMS disagreement of 1.3 m s^{-1} using the NASA scatterometer (NSCAT) and hourly observations of National Data Buoy Center (NDBC) buoys. Ebuchi et al. (2002) used almost 1.5 years of QuikSCAT observations together with the aforementioned hourly observations of the NDBC buoys, as well as 3-hourly, hourly, and every-10-min observations from other buoys, and obtained an RMS of 1 m s^{-1} . A more local study at the U.S. West Coast by Pickett et al. (2003) showed an RMS of 1 m s^{-1} for the first 17 months of QuikSCAT, by using a subset of the NDBC buoys with hourly observations. None of these studies performed additional temporal averaging. Bentamy et al. (2008) published one of the first studies using the first 8 months of ASCAT data together with the hourly NDBC buoy observations and hourly averaged observations from the Tropical Atmosphere Ocean (TAO) project. They showed

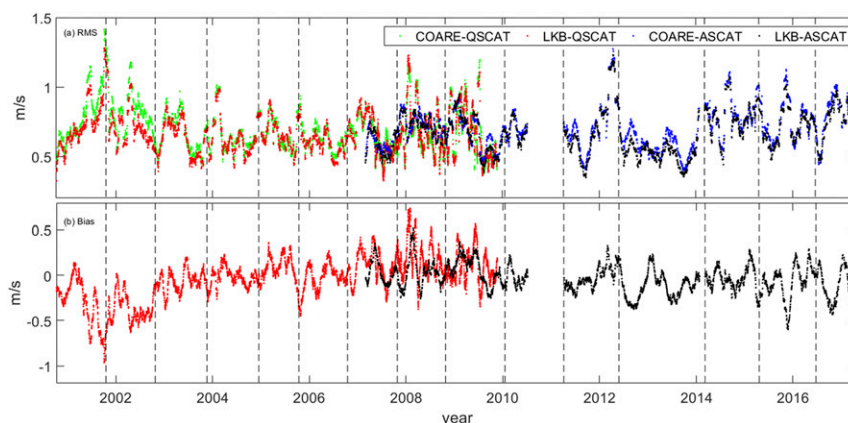


FIG. 1. (a) RMS difference between Stratus and QuikSCAT (red and green lines) and ASCAT (black and blue lines). The Stratus equivalent neutral winds were estimated with the COARE (green and blue) and LKB (red and black) parameterizations. The RMS differences were computed over 48 consecutive matchups of buoy and scatterometer observations (cf. the last paragraph of section 2). (b) Bias between the buoy and scatterometers for the same 48-point intervals (only the LKB buoy wind is shown). Note that the buoy design considered here was used only after 2004.

an RMS range of $0.65\text{--}1.72\text{ m s}^{-1}$ depending on which buoy array and which wind ranges are used. These results motivate a further analysis to get deeper insights into the intercomparison between buoy and scatterometer observations.

Generally, for all scatterometers wind speed, direction, and vector components are validated against buoys on a monthly basis from 3 months after launch by the Ocean and Sea Ice Satellite Application Facility (OSISAF) at the Royal Netherlands Meteorological Institute (KNMI). An approach for separately attributing the measurement errors to the different sources of wind observations is the triple collocation approach by Stoffelen (1998). With this approach, the errors of buoys, scatterometers and models are elaborated, as shown by a variety of studies (e.g., Vogelzang et al. 2011; Lin et al. 2015b; Stoffelen et al. 2017).

This work focuses on using the redundant, high-frequency (1-min average) buoy anemometer records together with independent scatterometer data to better understand the uncertainty and sources of error in the buoy wind measurements. As a first step, data from a site in the southeast Pacific were collocated with QuikSCAT and ASCAT observations. The buoy data were converted to 10-m-equivalent neutral wind speeds with two parameterizations, COARE3.0 (Fairall et al. 2003) and the Liu and Tang (1996) version of the Liu–Katsaros–Businger (LKB) parameterization (Liu et al. 1979). Generally, the two independent observations show an RMS difference between Stratus and QuikSCAT, as well as between Stratus and ASCAT, which is variable with time over the whole matching period (Fig. 1a). The

mean RMS when comparing to QuikSCAT is 0.71 m s^{-1} (10.2%) when using COARE and 0.68 m s^{-1} (9.6%) when using LKB. The mean RMS when comparing with ASCAT is 0.72 m s^{-1} (10.2%) with COARE, and 0.70 m s^{-1} (9.6%) with the LKB parameterization. Two more buoys [WHOI Hawaii Ocean Time series (HOT) Station (WHOTS) and Northwest Tropical Atlantic Station (NTAS)] are used in this paper, which were similarly compared with the scatterometers resulting in RMS of 0.76 (0.68) m s^{-1} for WHOTS–QuikSCAT with the COARE (LKB) parameterization and RMS of 0.71 (0.66) m s^{-1} for WHOTS–ASCAT. For the NTAS buoy we found RMS as low as 0.62 (0.56) m s^{-1} , when converted with COARE (LKB) and compared with QuikSCAT. For NTAS–ASCAT the RMSs are 0.60 (0.57) m s^{-1} . A similar temporal evolution can be seen for all buoys, but the temporal dependence of the RMS is not the focus of this paper. In this paper, we focus on the systematic errors caused by flow distortion around the buoy and its superstructure.

The bias between Stratus and QuikSCAT (Fig. 1b) exhibits appreciable variability over time, but this seems to be mostly attributable to variations in the quality of the buoy data. The largest negative values of the buoy–scatterometer bias occur in the first few Stratus deployments, when we were using a different buoy and superstructure design (a 3-m discus buoy) than the one that is the focus here. (We exclude those deployments from the analysis here.) The largest positive values on the bias occur in 2008, a time when both of the primary anemometers had failed on the Stratus buoy. (The time

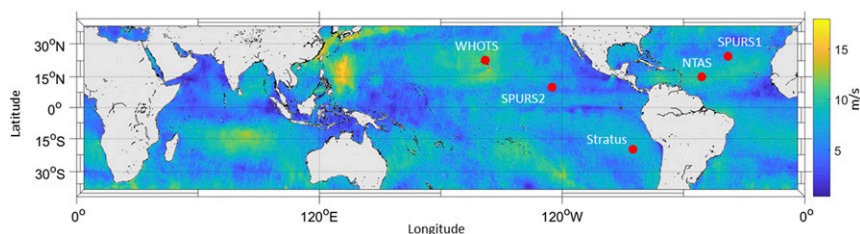


FIG. 2. Mean wind speed in the global tropical and subtropical ocean as seen from ASCAT on 21 Oct 2017. The red dots show the sites of the three ocean reference stations (WHOTS, NTAS, and Stratus) and the two SPURS sites.

series was patched with data from a third, backup anemometer, but the data from this deployment were not included in the flow-distortion analysis here.) Aside from those two periods, the mean buoy–scatterometer disagreement appears to be stable over time. Comparisons for the other buoys were similarly stable.

This paper is organized as follows. In [section 2](#), the buoy sites, data, and methods are presented, followed by the flow distortion analysis and the comparisons between buoy and scatterometer estimates in [section 3](#). Discussion and conclusions are given in [section 4](#).

2. Data and methods

a. Buoy sites

The WHOI UOP Group currently operates three ocean reference stations (ORS): Stratus off northern Chile in the eastern South Pacific, NTAS in the northern tropical Atlantic, and, coordinated with the HOT project, the WHOTS north of Oahu, Hawaii. Each ORS is maintained over many years by successive recovery of the deployed mooring and replacement with a refurbished mooring. Mooring replacements are nominally at 1-yr intervals. In addition to the ORS, two buoys were deployed for 15 and 12 months as part of the Salinity Processes in the Upper Ocean Regional Study (SPURS) project ([Fig. 2](#); details to all buoys in [Table 1](#)). The surface moorings are anchored to the seafloor, but the scope of the mooring allows the buoy to move within 7 km of its anchor position under the influence of currents and the wind around the anchor location.

Buoy positions are tracked using GPS or other satellite systems.

Stratus is moored in the eastern tropical Pacific 1100 km of the coast of Chile, in a region characterized by a persistent stratus cloud deck, for the purposes of observing and understanding regional air–sea interactions, providing independent surface and ocean observations to motivate improvements to ocean, atmospheric, and coupled models and calibrating and validating meteorological, air–sea flux, and ocean products derived from models, remote sensing methods or combinations of models and remote sensing ([Colbo and Weller 2007](#); [Weller 2015](#)).

NTAS is moored in a region of the tropical Atlantic with strong SST anomalies and the likelihood of significant local air–sea interaction. The primary science objectives of the NTAS project are to determine the in situ fluxes of heat, moisture, and momentum, and then to use these in situ fluxes to make a regional assessment of flux components from numerical weather prediction models and satellites.

The goal of WHOTS is to provide long-term, high-quality air–sea fluxes as a coordinated part of the HOT program, and contribute to the HOT goals of observing heat, momentum, freshwater and chemical fluxes at a site representative of the oligotrophic North Pacific Ocean.

The first SPURS deployment was in the salinity maximum region in the subtropical North Atlantic ([Farrar et al. 2015](#)), while the second SPURS deployment was in the low surface salinity belt in the eastern

TABLE 1. Overview of the buoys. Approximate locations are given. The exact location of the anchor varies slightly from one deployment to the next.

Buoy	Lat	Lon	Operation period	No. of deployments	
				All	Used for flow distortion
Stratus	20°S	85°W	Oct 2000–present	15	7
NTAS	15°N	51°W	Mar 2001–present	15	7
WHOTS	22°45′N	158°W	Aug 2004–present	13	7
SPURS 1	24°30′N	38°W	Sep 2012–Sep 2013	1	1
SPURS 2	10°N	125°W	Aug 2016–Nov 2017	1	0

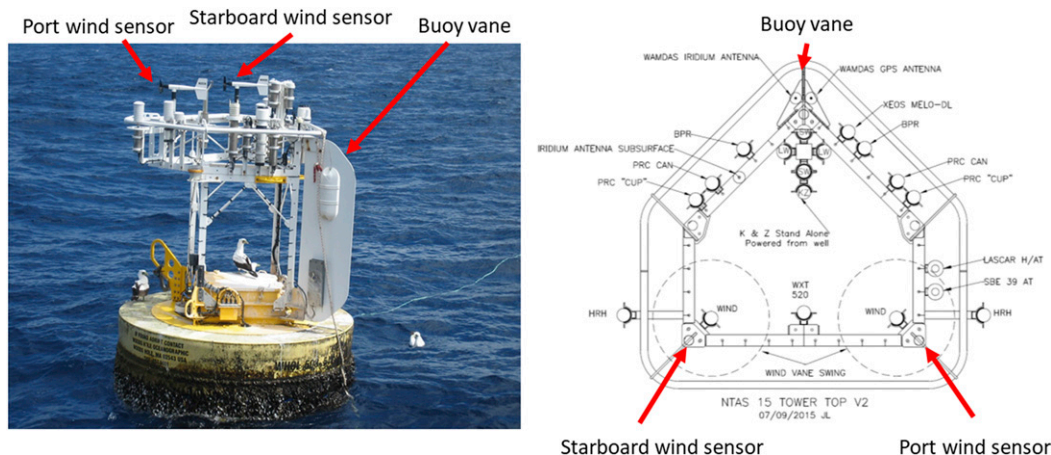


FIG. 3. (left) The Stratus buoy before recovery from its thirteenth deployment and (right) the NTAS buoy schematic for its fifteenth deployment (top view). Aluminum tubing forms an outer protective perimeter or “crash bar” to absorb contacts with the ship’s hull. Two humidity–temperature sensors (HRH) are outboard of the crash bar but the anemometers are inboard on the forward face, with the arc of the swing of the anemometers’ vanes inside the crash bar. In the center of the buoy is the storage well housing batteries and electronics.

tropical Pacific, related to the heavy rainfall within the ITCZ (Farrar and Plueddemann 2019).

b. Buoy instrumentation and physical configuration

All the aforementioned buoys are fully instrumented with either two Improved Meteorology (IMET) or two Air–Sea Interaction Meteorology (ASIMET) packages consisting of a suite of sensors each packaged together with their signal conditioning electronics and referred to as “modules” connected to power and to a datalogger and satellite data telemetry system. The sensor suite usually includes a module for relative humidity and air temperature (Rotronic MP-101A), a barometric pressure module (Heise DXD), a precipitation module (RM Young 50202), a module for shortwave radiation (Eppley Precision Spectral Pyranometer), a module for longwave radiation (Eppley Precision Infrared Radiometer), and a module for wind speed and direction, which can be either an RM Young propeller and vane anemometer (model 5103) or a Gill Sonic anemometer. To obtain the SST a Seabird model SBE37 mounted at about 1-m depth below the buoy is used. In most deployments, a third anemometer, a stand-alone sensor self-contained with battery power and data logging, has been deployed.

All the modules are mounted at different locations on the buoy (Fig. 3). The modules for air temperature, humidity, barometric pressure, and the rain gauges are mounted on the forward face of the upper frame. Placement of these sensors is aimed at positioning them in airflow that is as undisturbed as possible, while not positioning them outboard of a tubular “crash bar” that protects the tower and its sensors from encounters with

the ship’s hull during deployment and recovery. In part, as mentioned earlier, the attempt to position them in undisturbed air is accomplished by the vane that steers the buoy with respect to the wind. The radiation modules are mounted as high as possible to avoid any shadows or obstructions in their field of view. The SST and current sensors are mounted below the water line on the buoy bridle. The two wind modules attached to the ASIMET loggers are mounted on opposite sides on the forward face, opposite the buoy vane, to avoid as much flow distortion as possible. We will use the terms “port” and “starboard” to distinguish between the two wind modules, defining the buoy reference frame in analogy to a ship. The buoy’s wind vane is on the “stern” and the opposite side of the buoy, where the anemometers are mounted, is the “bow.” When looking from the stern to the bow, the buoy’s port side is to the left and the buoy’s starboard side is to the right.

When an RM Young vane/propeller module is used for wind observations, the wind is measured in 5-s segments, collecting total propeller rotations over the 5 s, one vane measurement each second, and a single snapshot of the compass value during these 5 s. For each 5-s segment, a vector average is formed from the 5-s-average vane and single snapshot compass. Eleven of these 5-s segments are vector averaged at the end of the 1-min interval to form the final vector velocity output. A 1-min scalar average of wind speed is also computed from the rotations of the propellers. After every minute the following variables are stored: the vector sum of 5-s velocities, the scalar-averaged wind speed, the maximum of the (5 s) wind speeds, the last vane direction, and the last compass direction.

When a sonic anemometer is used, the following sampling scheme is applied: Each measurement takes 25 ms, so the base sampling rate is 40 Hz. There is overhead involved to output the data at the end of a sampling burst, resulting in 195 samples in a 5-s interval (39 Hz). Within each 5-s interval the compass is polled once, near the center of the interval. One-minute averages are computed from eleven 5-s intervals with 5 s of overhead for vector averaging. At the end of every minute the following variables are stored: wind vector, scalar-averaged wind, maximum 5-s wind speed, minimum 5-s wind speed, last X – Y direction, last compass direction, x -axis tilt, and y -axis tilt (where X and Y are axes in the instrument frame of reference).

c. Buoy data

The data from the redundant instruments on the buoys are quality controlled to eventually provide one best-estimate dataset. For the ORS, where sequential 1-yr deployments of surface moorings have been made to collect ongoing, long-term time series, the typical approach is to deploy a new surface mooring in the vicinity of the existing mooring and collect one or more overlapping days of data. At the same time surface meteorological data are collected from the ship used to service the mooring and, whenever possible, one or more days of comparisons between the shipboard surface meteorology and the buoy observations are made with the ship stationed downwind of the buoy, bow into the wind. This results, for each deployment, in overlapping buoy data (old and new) and shipboard data. The sensors on the freshly deployed buoy were calibrated before the buoy was built, and the assembled buoy was run as a system both at WHOI and in port just prior to loading on the ship. These “burn-in” data were scrutinized and used to identify and correct any initial problems in sensor performance. After recovery, the sensors were returned for postdeployment calibration.

The 1-min data from the recovered buoy were collected together with hourly averaged telemetered data from the new buoy (access to the 1-min data is possible only by downloading from the datalogger), the shipboard data, and data from the European Centre for Medium-Range Weather Forecasts (ECMWF) operational model at grid points near the buoy. The overlapping buoy and ship data were examined to guide correction of any drifts in the recovered buoy data and the selection of the “best” time series. For many studies the goal is to create one high-quality, full-length record from the redundant sensors. Therefore, for both the ORS and the SPURS deployments,

postprocessing developed the best corrected time series from both of the buoy systems as well as the best single, complete surface meteorological dataset. A detailed description about data evaluation and postprocessing is given in [Bigorre and Galbraith \(2018\)](#).

For this study, we take advantage of the redundant sensors and the raw data of the wind vector, compass, and vane were used as well as the 1-min vector-averaged winds, and both the port and starboard wind records were employed. Air humidity and temperature, SST, and the ocean currents were also used. Ocean currents come from the shallowest useful data from a current meter deployed on the mooring line, allowing absolute and relative (i.e., relative to the currents) wind speeds to be estimated for the port and the starboard sensors. Furthermore, the absolute wind direction and the wind direction relative to the buoy heading can be estimated. The wind module vane angle is measured relative to the buoy heading, and the wind module compass measures the buoy heading—the sum of these gives the absolute wind direction. To examine the flow distortion, relative differences are calculated. The difference of the wind speed of the two sensors is normalized by the wind speed by one of the two sensors itself to estimate the percentage difference. Because the errors are a small fraction of the total wind speed, either sensor can be the divisor. Raw data for wind observations (wind vector, scalar wind, vane, compass) that were obviously spurious were discarded manually when they met any of the following criteria: wind vector components or scalar wind speeds exactly zero, vane and compass directions higher than 400° , and vane and compass directions lower than -10° . While wind observations of exactly 0 m s^{-1} are extremely unlikely, vane and compass observations are only reasonable between 0° and 360° . These quality-controlled data were further used either directly for intercomparison or converted to equivalent neutral winds.

To compare the wind with satellite estimates, equivalent neutral wind speeds were computed using two parameterizations as described above. The main reason for considering LKB here is that it is still the standard parameterization for the calculation of wind data from scatterometer estimates. Both parameterizations require the same data: wind components, air temperature, and air humidity with its respective measurement heights; SST, and surface current components. However, the COARE parameterization can utilize additional inputs (barometric pressure and net solar and infrared radiation) to, for example, estimate the ocean skin temperature. After several iterations a final roughness length and friction velocity is estimated. With these the turbulent fluxes; transfer coefficients for

momentum, latent heat, and sensible heat; and the equivalent neutral wind can be calculated.

d. Scatterometer data

Two datasets of scatterometer observations are used in this study, both provided by Remote Sensing Systems (RSS). The first one is from the SeaWinds scatterometer on the QuikSCAT satellite (“QuikSCAT” is used to refer to the scatterometer here). QuikSCAT is a scanning pencil-beam scatterometer, which was spinning from 19 July 1999 through 19 November 2009. We used the daily gridded data files on a 0.25° longitude \times 0.25° latitude grid (Ricciardulli et al. 2011). Rain-flagged data were discarded. Two observations per day (one on an ascending swath and one on a descending swath) are possible and due to the sun-synchronous orbit the local equator crossing time is nearly constant at 0600 LT for the ascending node and 1800 LT for the descending node. To get equivalent neutral winds they used their current GMF: “QuikSCAT Ku-201” (Ricciardulli and Wentz 2015). Note, that there are other Ku-band GMFs from other data providers. Wang et al. (2017b) recently presented a new GMF for Ku band, which corrects for SSTs, named NSCAT-5. Another GMF, which accounts for SSTs, is used for RapidSCAT, a scatterometer mounted on the International Space Station (ISS). This GMF is called KuSST and is an extension of the Ku-2011 GMF mentioned before.

The second scatterometer data product is ASCAT-A, also obtained from RSS. Note, there are several different products with different quality using the same original data (e.g., Wang et al. 2019). ASCAT is a scatterometer onboard the *MetOp-A* satellite and operating in C band. The first data are available from 1 March 2007 and it is still operating. As for QuikSCAT we used the daily data files on a 0.25° longitude \times 0.25° latitude grid (Ricciardulli and Wentz 2016) and discarded rain-flagged data. Again, two observations per day are possible and the sun-synchronous orbit has nearly constant equator crossing times at 0930 LT for the ascending node and 2130 LT for the descending node. ASCAT-A is very stable over time at the three aforementioned ORS buoy sites (cf. Fig. 1b for Stratus).

e. Methods

A common issue in comparing two observations, which have different time and space resolution, is their collocation. Each of the 14 daily orbits around the globe is covered in about 90 min, in which a large area is observed in a short time. The gridded product that is used provides a time in minutes as well. The smallest time increment is about 6 min. The task is to match these satellite data to the buoy observation, which is within its

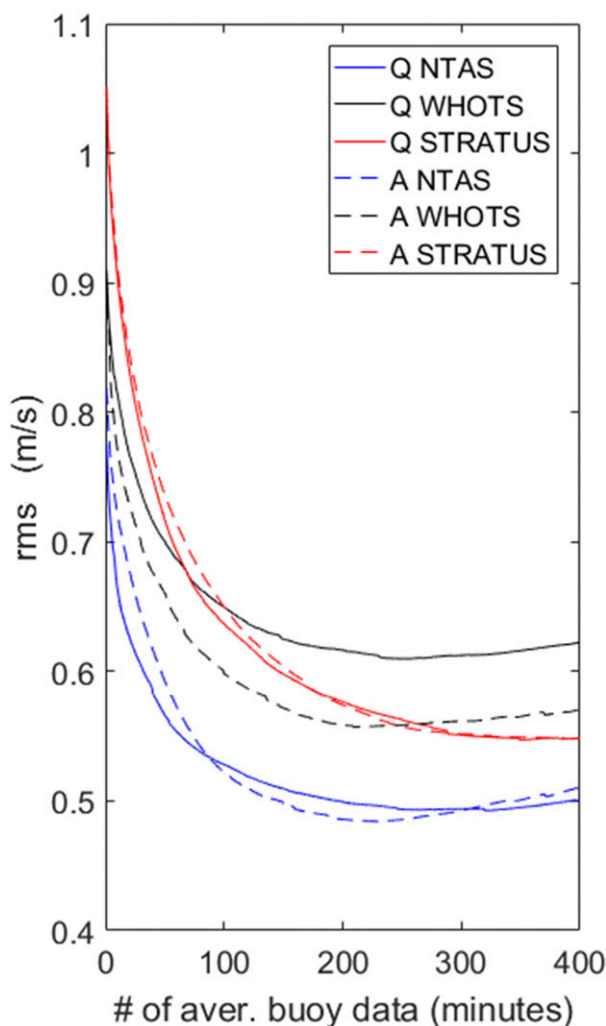


FIG. 4. Mean RMS between scatterometer and buoy against the averaging time of the buoy data. Averaging times between 1 and 400 min were used with 1-min increments. In the legend Q refers to QuikSCAT and A refers to ASCAT.

watch circle (~ 7 km) and has data at the resolution of 1 min. The satellite is matched to the nearest minute in time of the buoy time series and the closest grid point is used. Furthermore, the buoy data are averaged with a running mean over a specific time, as discussed below. The spatial representation can introduce a bias when comparing averaged wind vectors over a large area with local wind vectors.

The RMS between satellite and buoy wind speeds shows a dependence on the averaging time, regardless of which scatterometer or buoy is used (Fig. 4). All possible averaging times between 1 min (i.e., original resolution) and 400 min were used, subdivided in 1-min increments. Assuming a mean wind of 7 m s^{-1} , which is approximately the case for all considered buoy sites, this wind

covers approximately 25 km in an hour, which is the size of a region related to one grid point. However, the dynamic range of the wind is for wind speeds close to 0 m s^{-1} up to almost 20 m s^{-1} . Therefore, the averaging distance is not constant for a single averaging time. To account for this, we used the approach of Lin et al. (2015a) to estimate 25-km equivalent buoy winds. Specifically, for a scatterometer grid cell of $\Delta x = 25 \text{ km}$, we chose an averaging interval of $\Delta t = \Delta x/U$, where U is the wind vector average around the time of the satellite overpass with 1-min resolution and Δt is the sum of the time in 1-min increments. The summation is done until Δx reaches 25 km. The resulting averaging periods Δt range between 30 min and 7 h. We denote each averaged result a “buoy match” and those winds are used in this paper whenever a comparison between satellite and buoy data is shown.

We finally have time series of buoy observations of the wind vector from each sensor, the converted equivalent neutral wind speeds from each sensor (converted in the described way, not considering air mass density effects), and a time series of buoy matches, again separately for each sensor.

With the time series of buoy matches and scatterometer observations, RMS differences were computed. A period of 48 scatterometer–buoy matches was used for that; that is, 48 is the size of the window used for the RMS computation and represents 24.2 days on average (cf., e.g., Fig. 1a). RMSs are provided either by the actual value in units of wind speed (m s^{-1}) or as relative (%). The relative RMS is the quotient of the RMS and the averaged buoy wind speed over the considered period, multiplied by 100%.

3. Flow distortion

The first part of this section is about the flow distortion around the buoys with a few examples. The flow distortion at the buoy is investigated using the two wind observations at different positions on the buoy, port and starboard. The two sensors observe different wind speeds, while the true wind speed is not known.

The results of the CFD study (Emond et al. 2012) mentioned earlier will be introduced first. The study used a model mesh of the buoy that is comparable to the real buoys used in the ocean. The big advantage of a model study is, that the “true” wind is known and the “observed” wind at any arbitrary position on the model mesh can be compared to it. The tendency of the buoy to remain in a constant angle of about 30° relative to the flow for long times was accounted for the CFD study. When the buoy’s bow is oriented at 30° to the incident wind, the simulations showed a systematic positive wind

speed bias at the downstream wind sensor of about 3.5% and a negative bias at the upstream sensor of about 1% (Fig. 5). We will return to these results later when examining the buoy–scatterometer disagreements.

Using now the real buoy observations, first we present an example from the seventh deployment of the Stratus buoy. The time series of hourly averages of relative wind speeds of the two sensors agree quite well, indicating the general good performance of both sensors (Fig. 6a). The difference between them is generally below 0.3 m s^{-1} for the whole deployment period of more than one year (Fig. 6b). The absolute wind direction indicates a nearly constant regime of southeasterly winds, which are the trade winds in this part of the subtropical southeast Pacific (Fig. 6c). The wind directions of the two sensors are not the same. A dominant bias of around 10° is clearly visible, showing that the port sensor mostly observed more southerly wind directions (Fig. 6d). Changes in this difference usually occurred, when low wind speeds of less than 5 m s^{-1} were observed. These changes came along with changes or even jumps in the wind direction of both sensors. However, directional errors are not considered in this analysis.

Calculating the relative difference of wind speeds of the two sensors, a dependence on the wind direction relative to the buoy is obvious (Fig. 7). Generally, the buoy tends to move in both directions relative to the wind direction. This results from the interaction of either the buoy vane, which tries to align the buoy in the wind, and a torque, which follows from the wind action at the buoy storage well and the superstructure (Emond et al. 2012). Within a deviation of 50° to either side from the direction aligned with the buoy vane (0°), a linear relation can be observed. The relative difference is positive when subtracting the near-side observation from the far side; that is, when the wind blows from port direction (negative abscissa in Fig. 7) the difference of the starboard minus the port observation is positive. This linear dependence is valid for more than 80% of all deployments, regardless of the investigated buoy.

The seventh deployment of Stratus was chosen because it represents a “clean” example of a linear relation. The slope of the linear relation, the offset in the wind difference (i.e., the crossing of the y axis), the maximum bias, as well as the spread of the deviation of the buoy orientation from the relative north are different for each deployment. Generally, the range of the bias is about 5%, though can be up to 10% for a few deployments, but also can be smaller than 5% too. The range of angles, from which the wind impinges at the buoy, can differ from a couple of degrees to almost the full circle (180° from either side). Relative wind directions greater than 50° from one side are generally

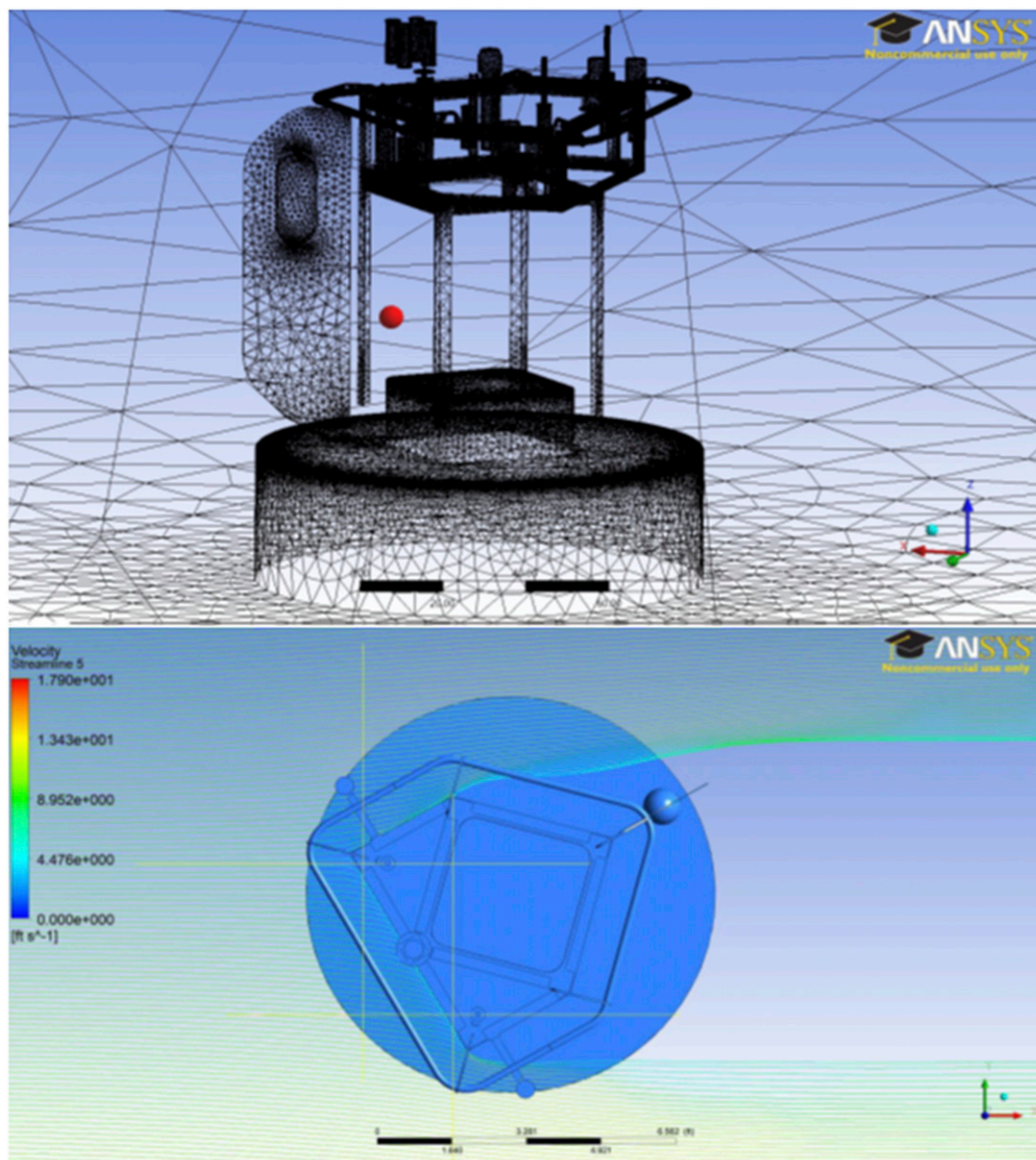


FIG. 5. (top) Model mesh of a WHOI buoy from the CFD study by Emond et al. (2012). (bottom) Streamlines around the buoy from the same study (top view). The yellow crosses are the wind sensor positions.

susceptible to additional errors, because the flow toward the far sensor can be significantly more distorted by the buoy superstructure or the upstream sensor itself. After several deployments the vane design was changed to a larger one and in the following deployments relative directions larger than 50° in either direction were rare, leading to a more stable position around the buoy north.

The satellite datasets from QuikSCAT and ASCAT are useful for getting insight into the disagreement between the two buoy anemometers. For the comparison with satellite observations, the buoy wind speeds were converted into equivalent neutral wind speeds. To

increase the amount of data, several deployments, at which the flow distortion behavior is similar, were analyzed together. Nevertheless, only deployments where the offset was close to zero, that is, the wind speed difference was zero at relative directions close to zero, were used. Slightly less than half (22 out of 45) of all deployments met these conditions (cf. rightmost column of Table 1). The remaining deployments show either no linear structure at all, which is mostly related to failure of one wind module, or they show a similar linear behavior between the two wind measurements, but exhibit some additional offset. At those deployments some additional source of uncertainty has an influence.

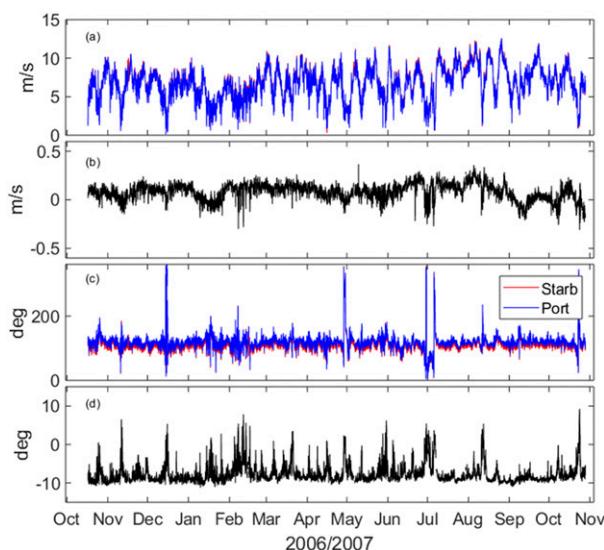


FIG. 6. Time series of Stratus's seventh deployment. (a) Wind speed of starboard (red) and port (blue) sensors, (b) the difference between them, (c) the wind direction of starboard (red) and port (blue) sensors, and (d) the difference between them. Shown are 1-h averages.

First, the Stratus deployments 4, 5, 6, and 7 were merged with the NTAS deployments 2, 4, 5, 6, and 8. These nine deployments are from a period when QuikSCAT was providing wind data and altogether consist of 4446 satellite–buoy matchups. This subsample of the buoy data can be plotted as a function of the wind incidence angle relative to the buoy in the same way as described before. A similar structure in the relative difference of the equivalent neutral wind speeds for all data is common. Using only the data of the matches with the QuikSCAT passes, the linear relation remains the same (Fig. 8a) for the wind directions between the buoy north and 50° from either side. This means that the subsample of the buoy data that is collocated with the satellite data is a good representation of the whole dataset. The probability distribution of the data shows a maximum close to the zero wind direction, slightly deviated to starboard winds, with small differences between the two modules (Fig. 8b).

Similar to the QuikSCAT period, the same was done for the ASCAT period. Here, the Stratus deployments 7, 11, 13, and 15 were merged with the NTAS deployments 8, 10, and 11, the WHOTS deployments 4, 5, 7, 10, 11, 12, and 13, and the first SPURS deployment. This led to 3832 matchups. The final figure with all ASCAT-matching data points again shows the linear relation (Fig. 8c). The probability distribution shows a symmetric structure with most of the data around zero relative wind direction (Fig. 8d). Both QuikSCAT and ASCAT results are consistent with the CFD flow simulations and

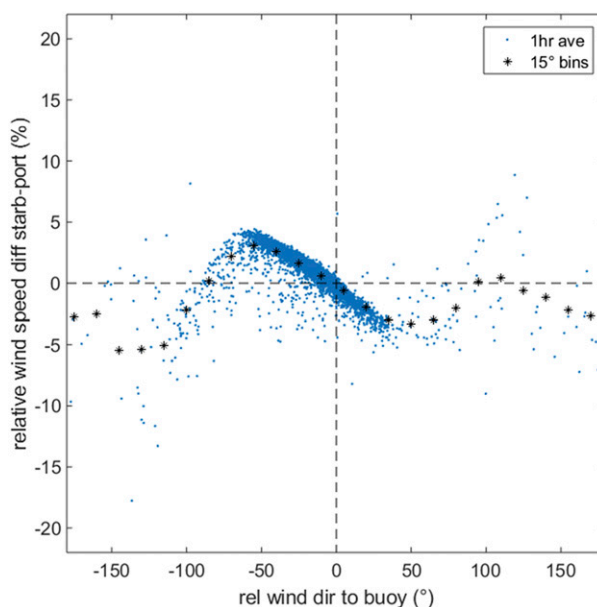


FIG. 7. Relative wind speed difference between starboard and port sensor for Stratus 7 against relative wind direction. Shown are 1-h averages (blue) and 15° -bin averages (black stars).

suggest a systematic error induced by the flow distortion around the buoy. This is true for all applicable datasets of redundant buoy observations, either the whole time series or the subset of scatterometer matches.

The CFD simulations predicted an asymmetric effect of flow distortion, with the upwind sensor having a negative wind speed bias that is slightly smaller than the positive wind speed bias on the downwind sensor. However, this asymmetry in the errors cannot be detected when examining the difference between the two sensors, because the differencing operations effectively combines the bias of the two sensors into a single number. Replacing one of the sensors with QuikSCAT or ASCAT observations enables us to possibly indicate the effect of the flow distortion. When plotted as a function of wind incidence angle in the buoy reference frame, the bin-averaged RMS difference between the buoy and scatterometer wind speeds resembles the comparison of port–starboard buoy anemometers (gray stars in Fig. 9). However, the linear relation between incidence angle and RMS disagreement is offset in the way that the average of the considered scatterometer data is always higher than the buoy average. This bias is about 1.1%, regardless which scatterometer product is used and compared to all considered buoy data. Taking the overall mean wind speed estimates from the scatterometers into account (QSCAT: 7.3 m s^{-1} ; ASCAT: 7.5 m s^{-1}), the absolute bias is about 0.08 m s^{-1} . This small bias could have many reasons, like atmospheric conditions, waves, or an additional effect of

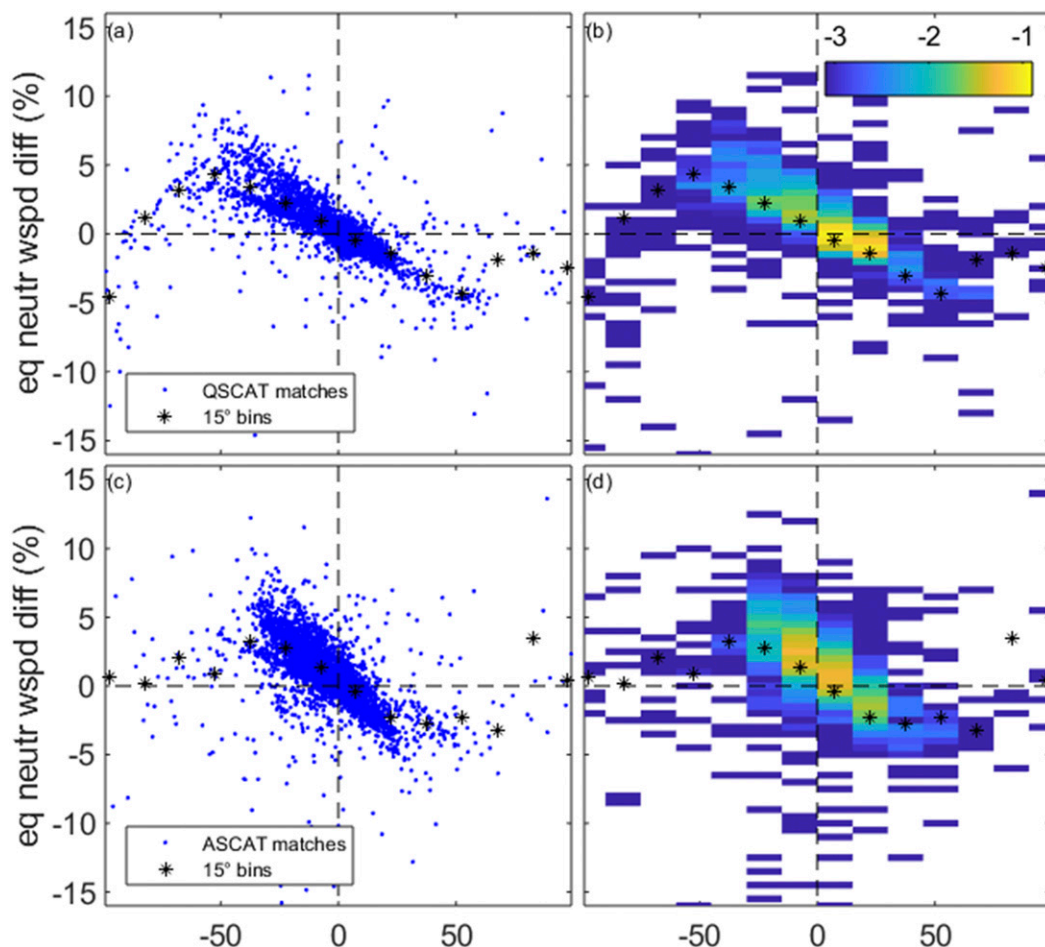


FIG. 8. Equivalent neutral wind speed difference between the starboard and the port sensor in relative percentage and against the relative wind direction. (a) All data that match with QSCAT (blue) and the bin averages of all data (black stars). (b) Probability distribution of the QSCAT matches within 15° bins (colors; shown is the logarithm to base 10) and corresponding bin averages (black stars). (c) All data that match with ASCAT (blue) and the bin averages of all data (black stars). (d) Probability distribution of the ASCAT matches within 15° bins (colors; shown is the logarithm to base 10) and corresponding bin averages (black stars).

flow distortion. Note, that the calibration of scatterometers against buoys to get a bias close to zero is done at the global average level. Somewhat arbitrarily, the offset was subtracted from the satellite time series (blue stars in Fig. 9). For incidence angles within $\pm 40^\circ$, the buoy–scatterometer differences are in good agreement with the CFD prediction by Emond et al. (2012)—the upwind sensor has a negative wind speed bias that is slightly lower than the positive bias seen on the downwind sensor (cf. to red crosses in Fig. 9).

Three lines of evidence—from the CFD simulations, from the port–starboard anemometer comparison, and from the scatterometer–buoy comparison—support the conclusion that there are flow distortion errors in the buoy wind speeds. Because these wind speed errors

seem to be a systematic function of the buoy incidence angle, we explored the possibility of making a correction to remove the flow distortion error from the module time series. Two attempts were made with the original time series of the two modules. The first approach was the application of the theoretical error between the two modules for the deviation of 30° on either side, as predicted by the CFD study. Emond et al. (2012) showed a relative error of +3.44% on the downwind side, and -1.03% on the upwind side. Applying this correction by linearly interpolating between -30° and 30° [the two largest angles used in Emond et al. (2012)] shows significant improvement in terms of the dependency of the module differences to the wind direction (red stars in Fig. 10). The second approach was using the same CFD

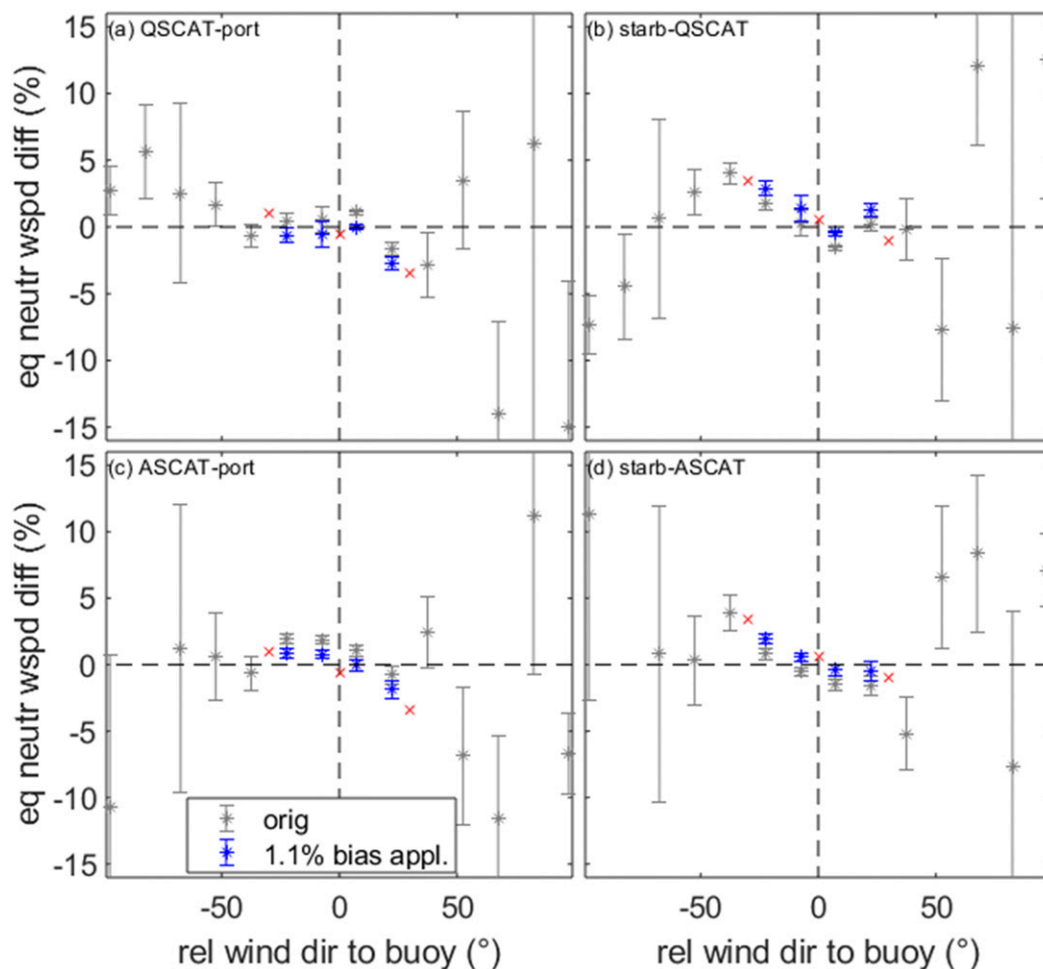


FIG. 9. Equivalent neutral wind speed differences, when replacing (a) the starboard module with QSCAT, (b) the port module with QuikSCAT, (c) the starboard module with ASCAT, and (d) the port module with ASCAT. Shown are the original bin averages (gray) and the bin averages within $\pm 30^\circ$ with 1.1% bias-corrected satellite data (blue). The red crosses indicate the theoretical flow distortion prediction as shown by Emond et al. (2012).

prediction, but applying the results to the observed error. This was done by using the error proportion at -30° and 30° from the CFD study (3.44% to -1.03%) to partition the port–starboard anemometer difference between the two anemometers. In the CFD study, the upwind anemometer was 1.03% low and the downwind anemometer was 3.44% high, so 23% of the interanemometer disagreement should be attributed to a low bias in the upwind anemometer and 77% should be attributed to a high bias in the downwind anemometer. This relation was then interpolated between -30° and 30° and applied to the observed error for every wind direction. The second correction appears to almost perfectly remove the flow distortion errors from the module time series (green stars in Fig. 10), but this is by construction because the mean interanemometer

disagreement at each angle is necessarily zero after application of this correction.

4. Discussion and conclusions

Wind observations from moored buoys were used in this study. Generally, those measurements are taken at about 3-m height on a platform (the buoy) that is moving in response to the wind, the waves, and the currents. Although wind measurements have been collected from buoys for many decades now, careful analysis is still needed to estimate and minimize the influence of errors.

a. Flow distortion

Flow distortion is one of these error sources. The influence of flow distortion was examined using different

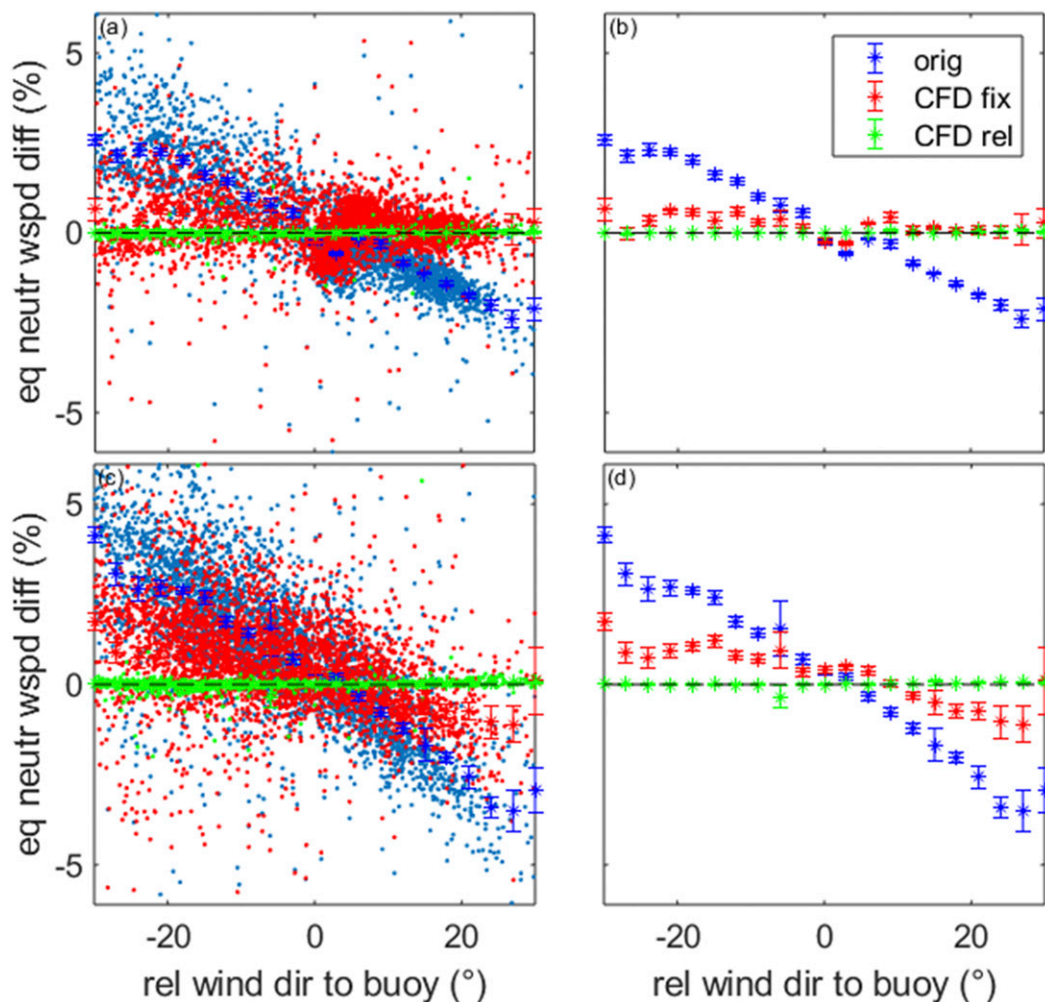


FIG. 10. Equivalent neutral wind speed difference (starboard minus port) from the QuikSCAT period. (a) Data from Fig. 6a (blue), after the fixed correction (red), and after the relative correction (green). (b) Corresponding bin averages from (a) in 3° bins. (c) As in (a), but for the ASCAT period and data from Fig. 6c (blue). (d) As in (b), for the ASCAT period.

WHOI buoys, and the relative disagreement of redundant anemometer wind speeds on the buoy reaches 5%, with a systematic dependence on the incidence angle of the wind relative to the buoy. For incidence angles within 50° of the buoy's bow, a linear relation is identified. This is valid for more than 80% of all deployments. Using half of the deployments (22 out of 45) that showed an interanemometer disagreement deemed "typical," the effect of flow distortion on the error could be estimated. This incidence-angle dependence is supported through comparison to measurements from scatterometers. We applied a correction for the flow distortion in the comparison between scatterometers and buoys. The dependence on the incidence angle almost disappears when the aforementioned bias of 1.1% and either of two flow distortion corrections based on the CFD simulations are applied (Fig. 11).

We are not aware of many published studies of flow distortion in wind measurements from oceanographic buoys. Similar results were estimated by Bigorre et al. (2013), using a much smaller dataset from the same type of buoy deployed in the Gulf Stream region. A CFD study has shown that the "faster" side of the buoy is high biased and the absolute value of this high bias is larger than the absolute value of the low bias on the "slower" side where the wind is coming from (Emond et al. 2012). The CFD simulations are certainly illuminating, but they were done for an idealized setting, with no wave motion or tilt on the buoy, and so we sought to also use independent datasets from QuikSCAT and ASCAT-A to try to assess the buoy errors.

All these results give an important overview over the systematic errors related to flow distortion and the

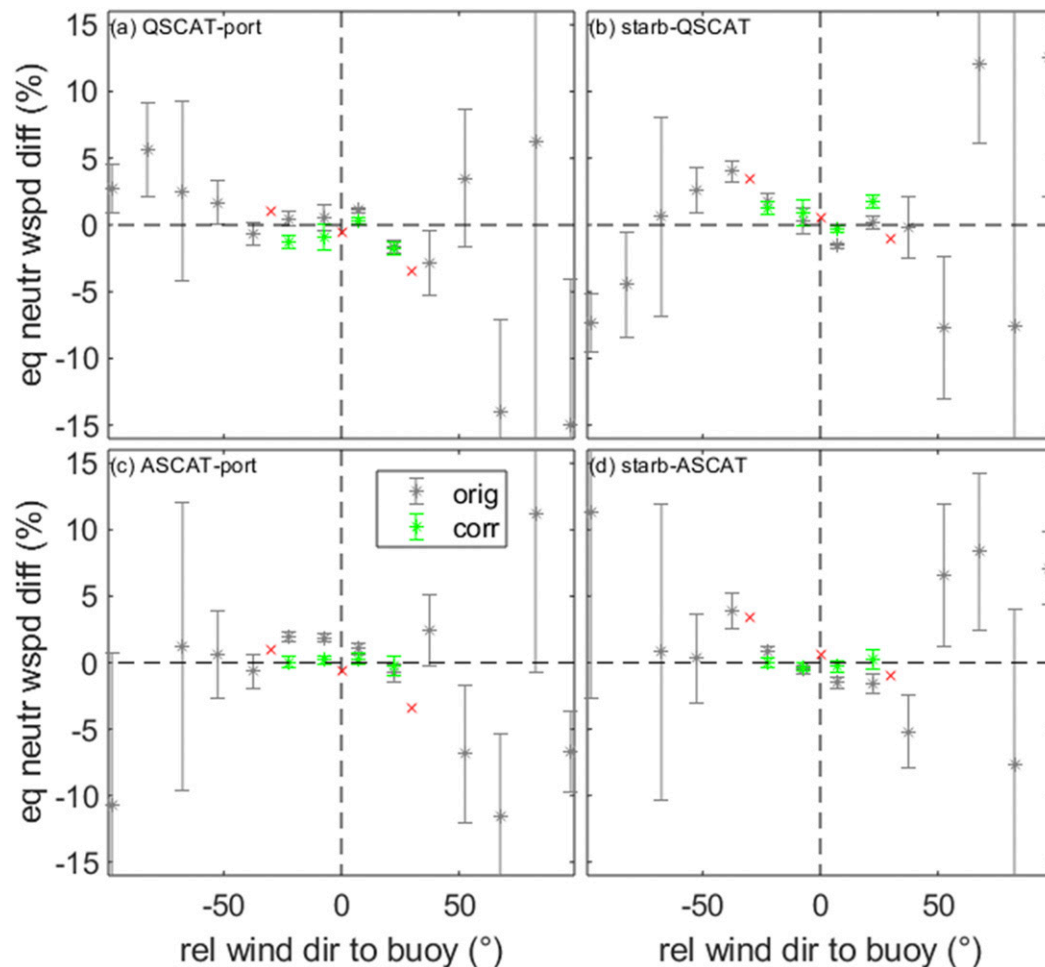


FIG. 11. As in Fig. 9, but with bias correction and relative flow distortion correction (green).

necessity to take them into account when using buoy observations as part of a ground truth for calibration and validation of satellite-based wind estimates.

b. Other error sources

It was also shown that the RMS between the equivalent neutral winds estimated from buoy observations and satellite measurements is as low as 0.5 m s^{-1} . Several additional aspects have to be considered when comparing direct wind observations on buoys with satellite-based estimates of near-surface winds.

1) CURRENTS

The scatterometer observes the sea surface, on which both the wind and the ocean itself act. Therefore, the scatterometer observes a wind relative to the surface currents. To compare them with buoy observations, the buoy wind has to be corrected for the currents to get relative winds. We used relative winds in this study, because all considered buoy deployments also observe

the near-surface currents. Therefore, the impact of surface currents on the error is expected to be negligible in this study.

2) COLLOCATION AND AVERAGING

One of the big issues is the collocation of the different independent data in space and time. Spatial and temporal representation errors are introduced by comparing averaged wind vectors over a large area (here 25 km) with local wind vectors. Stoffelen (1998) showed with a triple collocation approach, that the NOAA buoys have the largest error variance compared with scatterometers and an NCEP forecast model. May and Bourassa (2011) showed a nice approach of assessing the uncertainty between shipboard in situ data and scatterometer estimates. They deduced, that the main contribution to the total variance of the differences of collocated ship and scatterometer observations depends on the temporal difference between them. For differences less than 25 min, only the variances of the datasets itself need to

be considered, while the variance related to temporal and spatial differences needs to be accounted for differences greater than 25 min. This temporal difference between in situ and scatterometer observation is important for buoys also. We took advantage of the 1-min temporal resolution of the buoy data and compared in this study two approaches of collocating the different data types. One is the fixed-time averaging of the buoy time series, which would lead to 1-h averaging. The second approach is a variable averaging period described by [Lin et al. \(2015a\)](#). The wind speed is converted into a corresponding distance; this distance is added together over time until it reaches an equivalent of 25 km. The differences between the two approaches are small. The RMS differences with the second approach are slightly smaller, though, and eventually, the second approach was used. The spatiotemporal averaging of buoy and scatterometer is expected to be much more important when comparing scatterometers to buoys that do not have the 1-min temporal resolution that is available on WHOI buoys. For buoys with less temporal resolution, a collocation window of up to 30 min between buoy and scatterometer might still provide good estimates of buoy–scatterometer uncertainty.

3) VISCOSITY

A correction due to misrepresented viscosity, related to SSTs, was investigated following [Bentamy et al. \(2012\)](#) (not shown). In a recent paper, [Wang et al. \(2017a\)](#) showed the dependence of the SST effect on radar frequency, polarization, and the incidence angle. The temporal variations in water viscosity are important for scatterometers because this affects the wave behavior at the centimeter scales that dominate the radar backscatter. This only marginally reduces the RMS. While the viscosity is directly related to the SST, the effect of the viscosity is seasonally varying and can explain a portion of the variability in the RMS between buoys and scatterometers (cf. [Fig. 1](#)). However, this effect is only relevant in very cold waters and the viscosity correction was not applied to the scatterometer data.

4) GMF AND SCATTEROMETER ERRORS

The GMFs for Ku band are also SST dependent (see, e.g., [Wang et al. 2017b](#)), which is neglected in the Ku-2011 GMF used here. The SST varies at the Stratus site seasonally between 18° and 23°C, at NTAS between 25° and 29°C, and at WHOTS between 23° and 28°C. Furthermore, the Ku-band GMF is not directly related to stress, because it uses equivalent neutral winds at 10-m height. It misses the atmospheric mass density, mainly related to humidity ([de Kloe et al. 2017](#)). Following them, the air mass density varies between

1.16 and 1.22 kg m⁻³, yielding to wind speed differences ($u_{10s} - u_{10n}$) between 0 and -0.2 m s^{-1} . Therefore, the consideration of atmospheric mass density decreases the equivalent neutral wind speed in 10 m up to 0.2 m s^{-1} (seasonally varying).

Scatterometers itself exhibit some temporal variability in terms of their speeds, wind component statistics, and their differences with respect to buoys and models (e.g., [Verhoef et al. 2017](#)). However, the scatterometers used in this study are temporally stable over the considered time period.

5) SEASONAL CYCLES

Related to the aforementioned variability, seasonal cycles in the RMS are present as well (not shown). The seasonal cycle is similar at each buoy, but can differ strongly between sites. The seasonal cycles most likely result from other parameters and their seasonal evolution as described before. Unresolved gustiness is another possible source of seasonality. It was shown that scatterometers by themselves also observe a seasonality related to enhanced wind variability in the summer hemisphere ([Belmonte Rivas et al. 2017](#)). Moist convection can be one of the reasons for this. The temporal cycles of RMS differences are beyond the scope of this paper, but may be appropriate for a separate study.

Most of the time the RMS is about $0.56\text{--}0.76 \text{ m s}^{-1}$. The mentioned studies explain much of the differences between scatterometer and buoy observations of winds. Furthermore, [Lin et al. \(2015b\)](#) deduced that the comparison of buoys and scatterometers is largely determined by buoy location, data screening, and season. Generally, in situ observations on buoys and scatterometers, both different kinds of wind observations, show a consistent behavior over periods already longer than a decade. Therefore, both are very reliable by themselves. This highlights the continued importance of in situ point measurements from buoys for the purpose of scatterometer calibration. Furthermore, they can be used to validate gridded wind products. On the other hand, calibrated scatterometers can be used for spatial and temporal validation of reanalysis winds, as shown by, for example, [Belmonte Rivas and Stoffelen \(2019\)](#).

c. Conclusions

The influence of flow distortion was examined using different WHOI buoys together with scatterometer measurements. The relative disagreement of redundant anemometer wind speeds on the buoy can be up to 5% of the wind speed, with a systematic dependence on the incidence angle of the wind relative to the buoy. This is in agreement with expectations based on simulations of the flow distortion around the buoy

superstructures. The flow distortion errors can be corrected to some extent.

We have focused on the measurement errors in buoy winds, errors that exist despite efforts made by many people over several decades to identify and eliminate them. Scatterometers also have issues and biases that have also been the focus of sustained research and engineering efforts. Measurement errors from these instruments can be subtle and can change with time, and it is only by careful intercomparisons of independent measurements that we can be confident that we know the wind. A robust observing system for winds needs to include both buoys and scatterometers.

Acknowledgments. We gratefully acknowledge the help of three anonymous reviewers, whose input greatly improved the paper. In particular, one reviewer pointed out a mistake in our initial interpretation of scatterometer stability, which was corrected in the final manuscript. JTF and MS were supported by NASA Grant NNX14AM71G (International Ocean Vector Winds Science Team). The SPURS observations were supported by NASA (Grants NNX11AE84G, NNX15AG20G, and 80NSSC18K1494). The Stratus, NTAS, and WHOTS ocean reference stations (ORS) are long-term surface moorings deployed as part of the OceanSITES (<http://www.oceansites.org>) component of the Global Ocean Observing System, and are supported by NOAA's Climate Program Office's Ocean Observing and Monitoring Division, as are RAW, AJP, and SPB through the Cooperative Institute for the North Atlantic Region (CINAR) under Cooperative Agreement NA14OAR4320158 with NOAA Climate Program Office (CPO) (FundRef No. 100007298). The technical staff of the UOP Group at WHOI and the crews of NOAA and UNOLS vessels have been essential to the successful long-term maintenance of the ORS. Data availability statement: QuikSCAT and C-2015 ASCAT data are produced by Remote Sensing Systems and sponsored by the NASA Ocean Vector Winds Science Team. Data are available at www.remss.com.

REFERENCES

- Belmonte Rivas, M., and A. Stoffelen, 2019: Characterizing ERA-Interim and ERA5 surface wind biases using ASCAT. *Ocean Sci.*, **15**, 831–852, <https://doi.org/10.5194/os-15-831-2019>.
- , —, J. Verspeek, A. Verhoef, X. Neyt, and C. Anderson, 2017: Cone metrics: A new tool for the intercomparison of scatterometer records. *IEEE J. Sel. Top. Appl. Earth Obs. Remote Sens.*, **10**, 2195–2204, <https://doi.org/10.1109/JSTARS.2017.2647842>.
- Bentamy, A., D. Croize-Fillon, and C. Perigaud, 2008: Characterization of ASCAT measurements based on buoy and QuikSCAT wind vector observations. *Ocean Sci.*, **4**, 265–274, <https://doi.org/10.5194/os-4-265-2008>.
- , S. A. Grodsky, J. A. Carton, D. Croize-Fillon, and B. Chapron, 2012: Matching ASCAT and QuikSCAT winds. *J. Geophys. Res.*, **117**, C02011, <https://doi.org/10.1029/2011JC007479>.
- Bigorre, S. P., and N. R. Galbraith, 2018: Sensor performance and data quality control. *Observing the Oceans in Real Time*, R. Venkatesan et al., Eds., Springer, 243–261.
- , R. A. Weller, J. B. Edson, and J. D. Ware, 2013: A surface mooring for air–sea interaction research in the Gulf Stream. Part II: Analysis of the observations and their accuracies. *J. Atmos. Oceanic Technol.*, **30**, 450–469, <https://doi.org/10.1175/JTECH-D-12-00078.1>.
- Colbo, K., and R. Weller, 2007: The variability and heat budget of the upper ocean under the Chile-Peru stratus. *J. Mar. Res.*, **65**, 607–637, <https://doi.org/10.1357/002224007783649510>.
- , and —, 2009: Accuracy of the IMET sensor package in the subtropics. *J. Atmos. Oceanic Technol.*, **26**, 1867–1890, <https://doi.org/10.1175/2009JTECHO667.1>.
- de Kloe, J. D., A. Stoffelen, and A. Verhoef, 2017: Improved use of scatterometer measurements by using stress-equivalent reference winds. *IEEE J. Sel. Top. Appl. Earth Obs. Remote Sens.*, **10**, 2340–2347, <https://doi.org/10.1109/JSTARS.2017.2685242>.
- Ebuchi, N., H. C. Graber, and M. J. Caruso, 2002: Evaluation of wind vectors observed by QuikSCAT/SeaWinds using ocean buoy data. *J. Atmos. Oceanic Technol.*, **19**, 2049–2062, [https://doi.org/10.1175/1520-0426\(2002\)019<2049:EOWVOB>2.0.CO;2](https://doi.org/10.1175/1520-0426(2002)019<2049:EOWVOB>2.0.CO;2).
- Emond, M., D. Vandemark, J. Forsythe, A. J. Plueddemann, and J. T. Farrar, 2012: Flow distortion investigation of wind velocity perturbations for two ocean meteorological platforms. WHO Tech. Rep. WHOI-2012-02, 66 pp.
- Fairall, C. W., E. F. Bradley, J. E. Hare, A. A. Grachev, and J. B. Edson, 2003: Bulk parameterization of air–sea fluxes: Updates and verification for the COARE algorithm. *J. Climate*, **16**, 571–591, [https://doi.org/10.1175/1520-0442\(2003\)016<0571:BPOASF>2.0.CO;2](https://doi.org/10.1175/1520-0442(2003)016<0571:BPOASF>2.0.CO;2).
- Farrar, J. T., and A. J. Plueddemann, 2019: On the factors driving upper-ocean salinity variability at the western edge of the eastern Pacific fresh pool. *Oceanography*, **32** (2), 30–39, <https://doi.org/10.5670/OCEANOGRAPHY.2019.209>.
- , and Coauthors, 2015: Salinity and temperature balances at the SPURS central mooring during fall and winter. *Oceanography*, **28** (1), 56–65, <https://doi.org/10.5670/OCEANOGRAPHY.2015.06>.
- Figa-Saldaña, J., J. J. W. Wilson, E. Attema, R. Gelsthorpe, M. R. Drinkwater, and A. Stoffelen, 2002: The Advanced Scatterometer (ASCAT) on the Meteorological Operational (MetOp) platform: A follow on for European wind scatterometers. *Can. J. Remote Sens.*, **28**, 404–412, <https://doi.org/10.5589/m02-035>.
- Freilich, M. H., and R. S. Dunbar, 1999: The accuracy of the NSCAT 1 vector winds: Comparisons with National Data Buoy Center buoys. *J. Geophys. Res.*, **104**, 11 231–11 246, <https://doi.org/10.1029/1998JC900091>.
- Lin, W., M. Portabella, A. Stoffelen, A. Verhoef, and A. Turiel, 2015a: ASCAT wind quality control near rain. *IEEE Trans. Geosci. Remote Sens.*, **53**, 4165–4177, <https://doi.org/10.1109/TGRS.2015.2392372>.
- , —, —, J. Vogelzang, and A. Verhoef, 2015b: ASCAT wind quality under high subcell wind variability conditions. *J. Geophys. Res. Oceans*, **120**, 5804–5819, <https://doi.org/10.1002/2015JC010861>.
- Liu, W. T., and W. Tang, 1996: *Equivalent Neutral Wind*. JPL Publ. 96-17, 16 pp.
- , K. B. Katsaros, and J. A. Businger, 1979: Bulk parameterization of air–sea exchanges of heat and water vapor including

- the molecular constraints at the interface. *J. Atmos. Sci.*, **36**, 1722–1735, [https://doi.org/10.1175/1520-0469\(1979\)036<1722:BPOASE>2.0.CO;2](https://doi.org/10.1175/1520-0469(1979)036<1722:BPOASE>2.0.CO;2).
- Lungu, T., and P. S. Callahan, 2006: QuikSCAT science data product user's manual: Overview and geophysical data products, version 3. JPL Tech. Rep. D-18053-Rev A, 91 pp.
- May, J. C., and M. A. Bourassa, 2011: Quantifying variance due to temporal and spatial difference between ship and satellite winds. *J. Geophys. Res.*, **116**, C08013, <https://doi.org/10.1029/2010JC006931>.
- Pickett, M. H., W. Tang, L. K. Rosenfeld, and C. H. Wash, 2003: QuikSCAT satellite comparisons with nearshore buoy wind data off the U.S. West Coast. *J. Atmos. Oceanic Technol.*, **20**, 1869–1879, [https://doi.org/10.1175/1520-0426\(2003\)020<1869:QSCWNB>2.0.CO;2](https://doi.org/10.1175/1520-0426(2003)020<1869:QSCWNB>2.0.CO;2).
- Ricciardulli, L., and F. J. Wentz, 2015: A scatterometer geophysical model function for climate-quality winds: QuikSCAT Ku-2011. *J. Atmos. Oceanic Technol.*, **32**, 1829–1846, <https://doi.org/10.1175/JTECH-D-15-0008.1>.
- , and —, 2016: Remote sensing systems ASCAT C-2015 daily ocean vector winds on 0.25 deg grid, version 02.1. Remote Sensing Systems, accessed 16 May 2018, www.remss.com/missions/ascats.
- , —, and D. K. Smith, 2011: Remote sensing systems QuikSCAT Ku-2011 daily and weekly ocean vector winds on 0.25 deg grid, version 4. Remote Sensing Systems, accessed 16 May 2018, www.remss.com/missions/qscat.
- Stoffelen, A., 1998: Toward the true near-surface wind speed: Error modeling and calibration using triple collocation. *J. Geophys. Res.*, **103**, 7755–7766, <https://doi.org/10.1029/97JC03180>.
- , and M. Portabella, 2006: On Bayesian scatterometer wind inversion. *IEEE Trans. Geosci. Remote Sens.*, **44**, 1523–1533, <https://doi.org/10.1109/TGRS.2005.862502>.
- , J. A. Verspeek, J. Vogelzang, and A. Verhoef, 2017: The CMOD7 geophysical model function for ASCAT and ERS wind retrievals. *IEEE J. Sel. Top. Appl. Earth Obs. Remote Sens.*, **10**, 2123–2134, <https://doi.org/10.1109/JSTARS.2017.2681806>.
- Verhoef, A., J. Vogelzang, J. Verspeek, and A. Stoffelen, 2017: Long-term scatterometer wind climate data records. *IEEE J. Sel. Top. Appl. Earth Obs. Remote Sens.*, **10**, 2186–2194, <https://doi.org/10.1109/JSTARS.2016.2615873>.
- Vogelzang, J., A. Stoffelen, A. Verhoef, and J. Figa-Saldaña, 2011: On the quality of high-resolution scatterometer winds. *J. Geophys. Res.*, **116**, C10033, <https://doi.org/10.1029/2010JC006640>.
- Wang, Z., A. Stoffelen, F. Fois, A. Verhoef, C. Zhao, M. Lin, and G. Chen, 2017a: SST dependence of Ku- and C-band backscatter measurements. *IEEE J. Sel. Top. Appl. Earth Obs. Remote Sens.*, **10**, 2135–2146, <https://doi.org/10.1109/JSTARS.2016.2600749>.
- , —, C. Zhao, J. Vogelzang, A. Verhoef, J. Verspeek, M. Lin, and G. Chen, 2017b: An SST-dependent Ku-band geophysical model function for RapidScat. *J. Geophys. Res. Oceans*, **122**, 3461–3480, <https://doi.org/10.1002/2016JC012619>.
- , —, B. Zhang, Y. He, W. Lin, and X. Li, 2019: Inconsistencies in scatterometer wind products based on ASCAT and OSCAT-2 collocations. *Remote Sens. Environ.*, **225**, 207–216, <https://doi.org/10.1016/j.rse.2019.03.005>.
- Weissman, D. E., B. W. Stiles, S. M. Hristova-Veleva, D. G. Long, D. K. Smith, K. A. Hilburn, and W. L. Jones, 2012: Challenges to satellite sensors of ocean winds: Addressing precipitation effects. *J. Atmos. Oceanic Technol.*, **29**, 356–374, <https://doi.org/10.1175/JTECH-D-11-00054.1>.
- Weller, R. A., 2015: Variability and trends in surface meteorology and air–sea fluxes at a site off northern Chile. *J. Climate*, **28**, 3004–3023, <https://doi.org/10.1175/JCLI-D-14-00591.1>.
- Yu, L., and X. Jin, 2012: Buoy perspective of a high-resolution global ocean vector wind analysis constructed from passive radiometers and active scatterometers (1987–present). *J. Geophys. Res.*, **117**, C11013, <https://doi.org/10.1029/2012JC008069>.